Acta Technologica Agriculturae 2
Nitra, Slovaca Universitas Agriculturae Nitriae, 2025, pp. 105–116

RESPONSE OF DIFFERENT TYPES OF CHOCOLATE TO IMPACT LOADING – DIRECT IMPACT

Vojtěch KUMBÁR*[1], Jan TRNKA[2], Jiří VOTAVA[1], Veronika ŠAFRÁNKOVÁ[3], Renáta DUFKOVÁ[3], Martin FAJMAN[1], Jiří ČUPERA[1], Šárka NEDOMOVÁ[3], Luděk HŘIVNA[3], Jaroslav BUCHAR[1]

[1]Mendel University in Brno, Faculty of AgriSciences, Department of Technology and Automobile Transport, Brno, Czech Republic, jiri.votava@mendelu.cz (J.V.), martin.fajman@mendelu.cz (M.F.), jiri.cupera@mendelu.cz (J.Č.), jaroslav.buchar@mendelu.cz (J.B.)
[2]Czech Academy of Science, Institute of Thermomechanics, Prague, Czech Republic, trnka@it.cas.cz
[3]Mendel University in Brno, Faculty of AgriSciences, Department of Food Technology, Brno, Czech Republic, veronika.safrankova@mendelu.cz (V.Š.), renata.dufkova@mendelu.cz (R.D.), sarka.nedomova@mendelu.cz (Š.N.), ludek.hrivna@mendelu.cz (L.H.)

*correspondence: vojtech.kumbar@mendelu.cz

This study investigates the dynamic response of various chocolate types to direct impact at high strain rates, which has significant implications for practical applications such as production, packaging, and transportation. Five different chocolate types – extra dark, dark, milk, white, and ruby – were evaluated. Experiments were conducted using the Direct Impact Hopkinson Bar (DIHB) technique, which enables the study of the mechanical behaviour of materials at strain rates exceeding 10^3 s^{-1}. The influence of specimen length on the mechanical response of the chocolates was also examined. Impact responses were characterized in both the time and frequency domains. Results indicate that dark chocolate exhibited the highest resistance to impact loading. Furthermore, an enhancement in mechanical properties with increasing impact velocity was observed across all chocolate types.

Keywords: cocoa content; impact velocity; permanent strain; DIHB technique; frequency analysis

The mechanical behaviour of chocolate is predominantly studied at elevated temperatures when it is in the liquid state. The rheological properties in this state are critical for understanding and optimizing the chocolate production process, as chocolate is processed while molten (Talansier et al., 2019; Bhattacharyya and Joshi, 2022; Hendrik et al., 2023). Rheological studies typically present results in terms of shear stress and shear strain rates (Kiumarsi et al., 2017; Mohamad et al., 2020; Kumbár et al., 2021), with strain rates reaching values up to 100 s^{-1}. In the solid state, the mechanical behaviour of chocolate can be characterized by material properties such as Young's modulus, yield stress, and fracture stress (Zhao et al., 2018; Gómez et al., 2022; Bikos et al., 2023). As noted by Bikos et al. (2021), although many researchers have emphasized the viscoelastic behaviour of molten chocolate, there have been limited investigations into the rate dependency of its mechanical properties in the solid state (Baldino et al., 2010; Nedomová et al., 2013; Glicerina et al., 2013). In these studies, compression tests were performed at strain rates significantly lower than those in rheological experiments, typically between 0.001 and 1 s^{-1}. These strain rates are characteristic of oral processing activities such as mastication (Carvalho-da-Silva et al., 2011; Le Révérend et al., 2016). Results from these compression tests demonstrate a significant effect of these relatively low strain rates on the aforementioned mechanical properties. Mechanical properties may increase significantly at strain rates exceeding 10^2 s^{-1} (Shui-Sheng et al., 2013), corresponding to those achieved during the rheological tests of liquid chocolate. This hypothesis was confirmed by Kumbár et al. (2023), who studied the mechanical behaviour of chocolate at high strain rates using the Split Hopkinson Pressure Bar (SHPB) technique, achieving strain rates up to $2 \cdot 10^3$ s^{-1}. In the SHPB technique, a specimen is placed between an input and an output bar. The input bar is struck by a striker bar, transmitting a pressure stress pulse through the input bar into the specimen and then into the output bar. The bars remain elastic during the experiment, enabling the measurement of force and velocity histories at their ends, and consequently determining the specimen's response.

In the present study, a modification of this technique known as the Direct Impact Hopkinson Bar (DIHB) was employed. In the DIHB technique, the input bar is omitted, and the specimen is struck directly by the striker bar. Directly impacting the specimen offers several advantages over using an input bar, including access to higher strains and higher strain rates for equivalent striker velocities, reduced dispersion, and faster attainment of force equilibrium (Couque, 2014). This paper presents experimental data on the high strain rate behaviour of five different types of chocolate – extra dark, dark, milk, white, and ruby. This behaviour is characterized in both the time and frequency domains.

Material and Methods

Five types of chocolate masses were utilized in the experiments: extra dark chocolate (EDC), dark chocolate (DC), milk chocolate (MC), white chocolate (WC), and ruby chocolate (RC). The EDC, sourced from Domori (Italy), comprises 100% cocoa components originating from Morogoro, Tanzania. The DC, MC, and WC were obtained from Belcolade (Switzerland), containing the cocoa components of 55.5%, 36.5%, and 28%, respectively. The RC was procured from Callebaut (Belgium) and contains 47.3% cocoa components. Detailed characteristics – including processing technology, composition, and nutritional information – of these chocolate masses are documented in Kumbár et al. (2021). The mechanical properties of these chocolates have been studied at both low strain rates (Kumbár et al., 2021) and high strain rates (up to $2{\cdot}10^3$ s^{-1}) (Kumbár et al., 2023). Additionally, the acoustic properties of these chocolates were evaluated in Nedomová et al. (2023). The acoustic properties, specifically the velocities of longitudinal c_L and transverse c_T acoustic waves, were measured. A crucial parameter is the longitudinal wave velocity in an elastic bar under the assumption of uniaxial stress state, denoted as c_0. This velocity, also referred to as the bar velocity, is defined by the equation:

$$c_0 = \sqrt{\frac{E}{\rho}} \tag{1}$$

where: E – represents the Young's modulus of elasticity; ρ – the material density

The propagation of acoustic waves is characterized by the specific acoustic impedance:

$$Z = \rho \cdot c_0 \tag{2}$$

Owing to the significance of these parameters in describing dynamic loading conditions (see Kumbár et al., 2023), their values are presented in Table 1.

Specimens were prepared in the form of cylinders with a diameter of 14 mm and lengths of 1, 2, 3, 4, and 5 mm for the experiments. These specimens were loaded using the Direct Impact Hopkinson Bar (DIHB) technique (Markovsky et al., 2023), as schematically illustrated in Fig. 1.

In this setup, the specimen is placed at the end of an elastic bar and is struck by an impactor moving at a striker velocity V. The loading history $\sigma_I(t)$ is recorded using a strain gauge affixed to the Hopkinson bar. If the striker mass is sufficiently large to provide kinetic energy much greater than that dissipated through the plastic deformation of the specimen, the impact velocity can be considered constant during the test. The strain in specimen can then be expressed as:

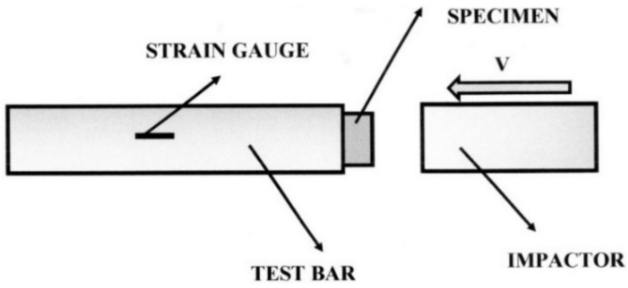

Fig. 1 The schematic of the Direct Impact Hopkinson Bar technique

$$\varepsilon(t) = \frac{u_2(t) - u_1(t)}{l_0} \tag{3}$$

where: $u_1(t)$ – denotes the displacement at the specimen-impactor interface; $u_2(t)$ – represents the displacement at the specimen-bar interface; l_0 – the initial length of the specimen

As detailed in Kumbár et al. (2024), these displacements can be expressed as:

$$u_1(t) = Vt - \frac{1}{Z_b}\int_0^t \sigma_T(t)dt \tag{4}$$

$$u_2(t) = -\frac{1}{Z_b}\int_0^t \sigma_T(t)dt \tag{5}$$

The strain rate is then given as:

$$\varepsilon(t) = \frac{2\int_0^t \sigma_T dt}{Z_b l_o} \tag{6}$$

where: l_0 – denotes the initial length of the specimen; σ_T – represents the stress recorded in the bar; Z_b – the acoustic impedance of the bar

The stress in the specimen is expressed as:

$$\sigma(t) = \sigma_T(t)\frac{A_T}{A_0} \tag{7}$$

Table 1 The acoustics characteristics of the tested chocolates

Chocolate	ρ (kg·m^{-3})	c_L (m·s^{-1})	c_T (m·s^{-1})	c_0 (m·s^{-1})	Z (MPa·s·m^{-1})
DC	1269.4	2208	798	1347.2	1.7102
MC	1263.4	2106	700	1187.0	1.4996
WC	1252.8	2094	649	1169.0	1.4645
RC	1244.8	2074	611	1103.6	1.3737
EDC	1170.0	1982	689	1039.4	1.2161

Here, A_0 and A_T denote the cross-sectional areas of the Hopkinson bar and the specimen, respectively. Corrections to Eq. (7) accounting for radial inertia effects are available in Guo et al. (2014) and Couque (2014). The impactor was fabricated from beech wood in the form of a cylinder with a diameter of 14.8 mm and a length of 152 mm. The elastic bar was constructed from polymethyl methacrylate (PMMA), also cylindrical, with a diameter of 15 mm and a length of 1000 mm. The acoustic impedance of the bar is Z_b = 2.6486 MPa·s·m^{-1}, and that of the impactor is Z_s = 3.42 MPa·s·m^{-1}. The specimen's response to impact loading is characterized by the time history of the stress wave $\sigma_I(t)$ recorded in the elastic bar. This stress pulse is defined by several parameters:

– the maximum stress (amplitude): σ_{Im},

– the impulse: $I_I = \int \sigma_I(t)dt$ (8)

– the energy: $W_I = \frac{1}{Z_b}\int \sigma_I^2(t)dt$ (9)

Additionally, the specimen's response to the stress pulse can be analyzed in the frequency domain, as discussed by Stein and Shakarchi (2003). This analysis involves an integral transformation that maps a time-domain function to its spectral function via:

$$S_I = \int_{-\infty}^{\infty} \sigma_I(t)e^{i\omega t}dt \quad (10)$$

where: ω – denotes the angular frequency

The spectral function is generally a complex quantity and can be expressed as:

$$S(\omega) = ReS(\omega) + ImS(\omega) = \sqrt{ReS(\omega)^2 + ImS(\omega)^2}\, e^{i\varphi} = Se^{i\varphi} \quad (11)$$

where: S – denotes the magnitude; φ – represents the phase of the spectral function

The chocolate specimens were subjected to stress pulses corresponding to three groups of striking velocities: 8 m·s^{-1}, 12 m·s^{-1}, and 16 m·s^{-1}. All experiments were conducted at a temperature of 12 °C, at which all tested chocolates behave as solid materials.

Results and Discussion

Initially, the specimen's response to impact loading was characterized by the permanent strain:

$$\varepsilon_p = \frac{\Delta l}{l_0} \quad (12)$$

where: $\Delta l = l_0 - l$. In this expression; l – represents the specimen's thickness measured after loading; l_0 – the initial specimen thickness, which was varied among 1, 2, 3, 4, and 5 mm. As illustrated in Fig. 2, the permanent strain increases with the impactor's striking velocity and decreases with increasing specimen length

For all striking velocities tested, the lowest permanent strain was observed in specimens made of dark chocolate. The ranking of tested chocolates according to permanent strain is as follows:

$$dark \rightarrow milk \rightarrow white \rightarrow extra\ dark \rightarrow ruby \quad (13)$$

The specimen's response to impact loading in the time domain is further characterized by the stress pulse $\sigma_I(t)$ recorded in the elastic bar. The time histories of this stress are presented in Fig. 3.

An examination of the recorded stress pulses reveals that their qualitative characteristics are consistently similar across all specimens. To gain a more detailed understanding of the specimen responses, the quantitative analysis of the stress pulse parameters was conducted.

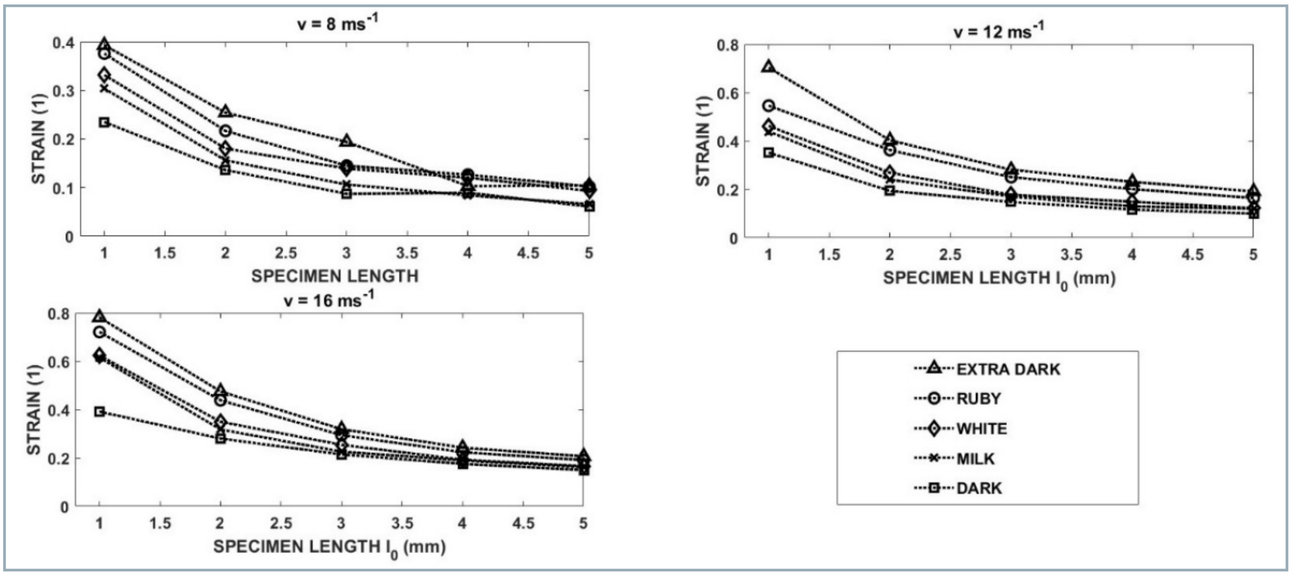

Fig. 2 The effect of the specimen length and striking velocity on the permanent strain of the chocolate specimens

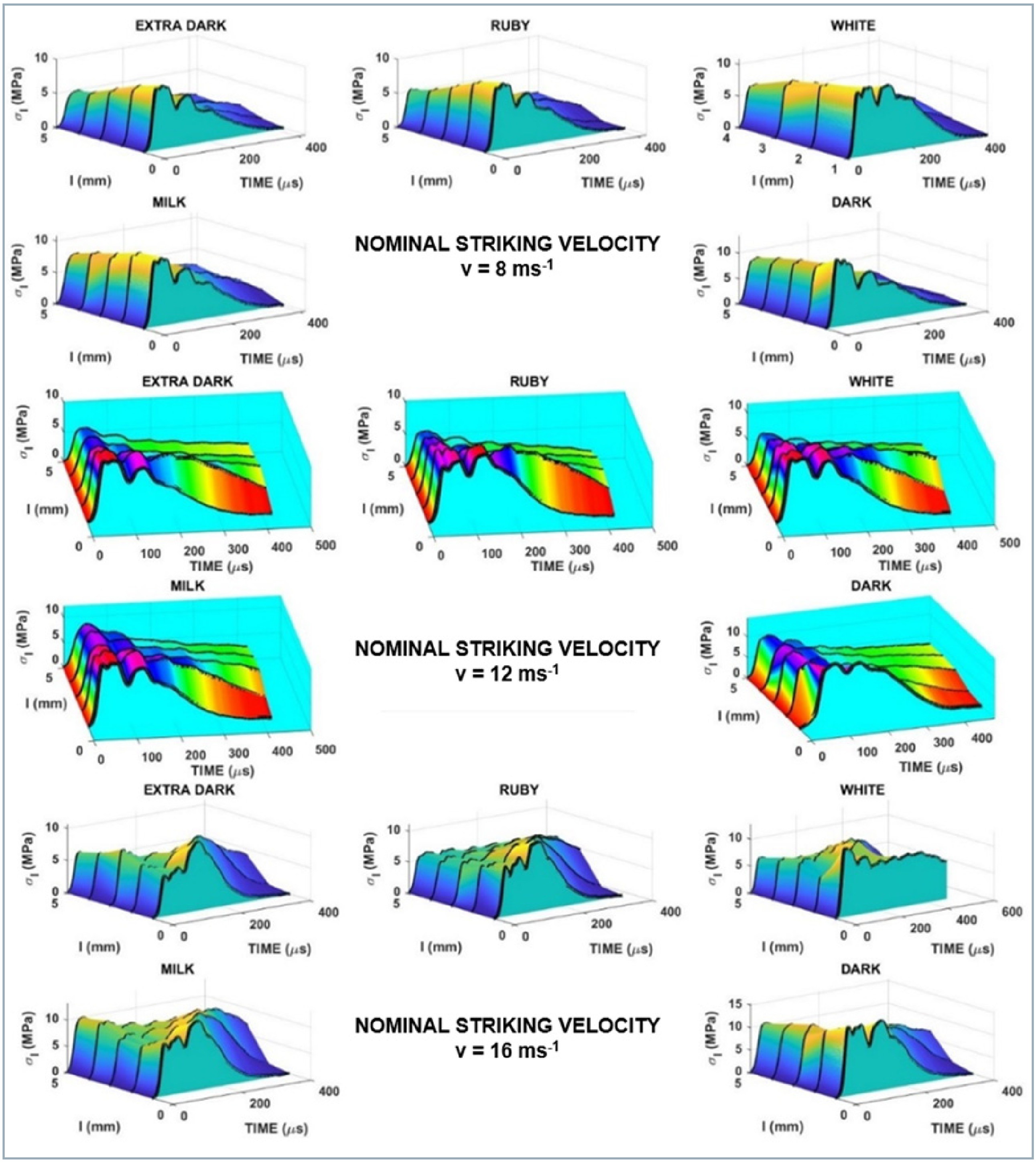

Fig. 3 The response of the chocolates to impact loading

Figure 4 presents an example illustrating the influence of the striker velocity v and the specimen length l_0 on the maximum amplitude of the stress pulse. The experimental data can be fitted by the linear function:

$$\sigma_l = a + b \cdot v + c \cdot l_0 \tag{14}$$

This conclusion holds true for all the tested chocolate varieties. The parameters associated with Eq. (14) are provided in Table 2.

The analysis of the data reveals that the amplitude of the stress pulse decreases with increasing specimen length. This attenuation is attributed to the evolution of permanent strain within the specimen, which dissipates energy from the stress wave. A similar effect was observed in our previous study (Kumbár et al., 2024) under different impact loading conditions. At a fixed specimen length, the stress pulse amplitude increases with the striking velocity *v*. The sensitivity of the stress pulse amplitude to the striking velocity, $\partial\sigma l)/\partial v$, is characterized by the parameter *b*, while

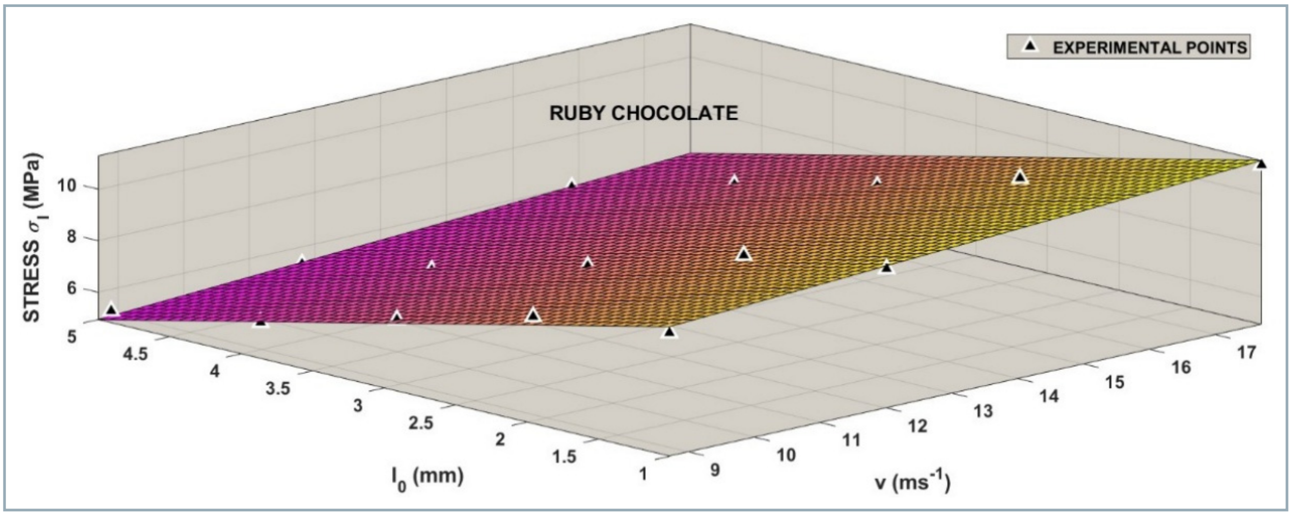

Fig. 4 The effect of the specimen length and striking velocity on the maximum of the stress transmitted through the specimen in the test bar

Table 2 The parameters of Eq. (2) (R2 denotes the coefficient of determination)

Chocolate	*a* (MPa)	*b* (MPa·s·m^{-1})	*c* (MPa·mm^{-1})	R^2
EDC	11.2265	0.0161	-1.2240	0.9025
RC	9.9455	0.1476	-1.2582	0.9905
WC	11.2739	0.1837	-1.4810	0.9558
MC	10.4190	0.2389	-0.9837	0.9809
DC	12.0120	0.2577	-1.1866	0.9574

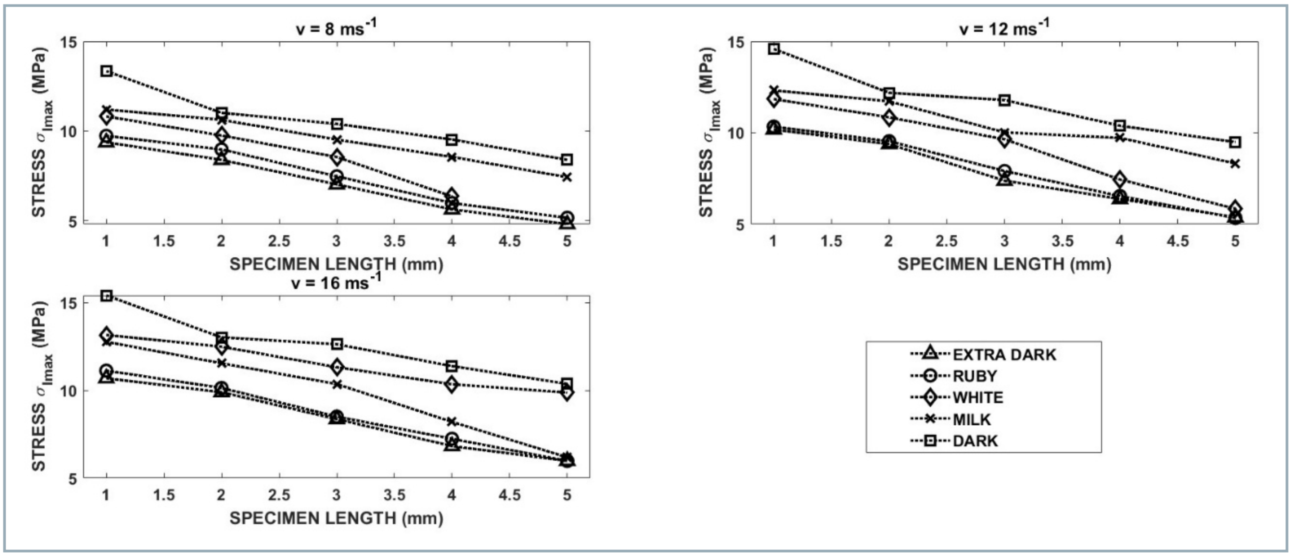

Fig. 5 The effect of chocolate type on specimen response for different values of the striking velocities

the parameter *c* quantifies the sensitivity to specimen length. The effect of chocolate type on the specimen's response to impact loading is illustrated in Fig. 5.

The ranking of the tested chocolates according to stress pulse amplitude is:

$$extra\ dark \rightarrow ruby \rightarrow white \rightarrow milk \rightarrow dark \qquad (15)$$

An equivalent ordering is observed when utilizing the parameter b, which quantifies the stress sensitivity to striking velocity. Furthermore, this consistent ranking of the tested chocolates is confirmed when analysing the specific acoustic impedance values provided in Table 1. To illustrate the effect of this parameter on the chocolate's response to the impact of a striker, we employ a simplified model wherein an infinite striker impacts an infinite, elastically behaving chocolate bar. The solution to this problem is provided by the theory of one-dimensional elastic wave propagation, as described in Wang et al. (2023). The maximum stress pulse in the chocolate bar is given by:

$$\sigma_{Im} = \frac{\beta}{\beta + 1} Z_b v \tag{16}$$

where: $\beta = \frac{A_s Z_s}{A_b Z_b}$, A – the cross-sectional area of the bar; Z – the acoustic impedance. The subscripts s and b correspond to the chocolate bar and the striking bar (beech bar), respectively; v – the striking velocity

The dependence of σ_I on v, as given by Eq. (16), is displayed in Fig. 6.

In Fig. 7, the stress values predicted by Eq. (16) are compared with our experimental data. It is evident that due to the development of plastic strain during our experiments, the most of the experimental stress values lie well below those predicted by Eq. (16). An exception is observed in the results obtained for the specimens of length 1–2 mm. This anomaly is a consequence of the transmission and reflection of stress waves within the specimen at the interfaces between the striker and the specimen, and between the specimen and the elastic bar; the details of this interaction are described in Wang et al. (2023). This ordering of chocolates is opposite to that determined by the permanent strain, as seen in Eq. (15). The smallest difference in the stress pulse amplitude values is observed between the extra dark and ruby chocolates.

When we examine the additional characteristics of the stress pulse – specifically, the impulse and energy – we observe that these parameters do not vary monotonically with specimen length. This is demonstrated by the examples presented in Fig. 8. It becomes apparent that the ranking of chocolates determined by Eq. (15) holds true only for specimen lengths ranging from 1 to 3 mm. Similar conclusions were drawn for the other striking velocities investigated.

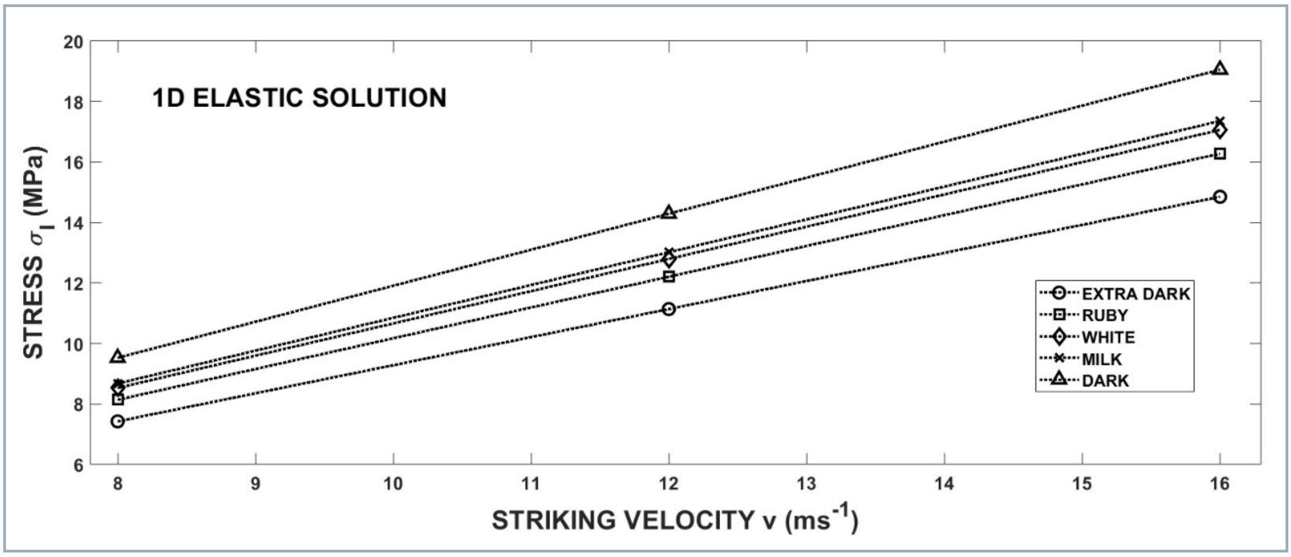

Fig. 6 The elastic response of the semi-infinite chocolate bar to the impact of the semi-infinite beech bar (1D theory of elasticity)

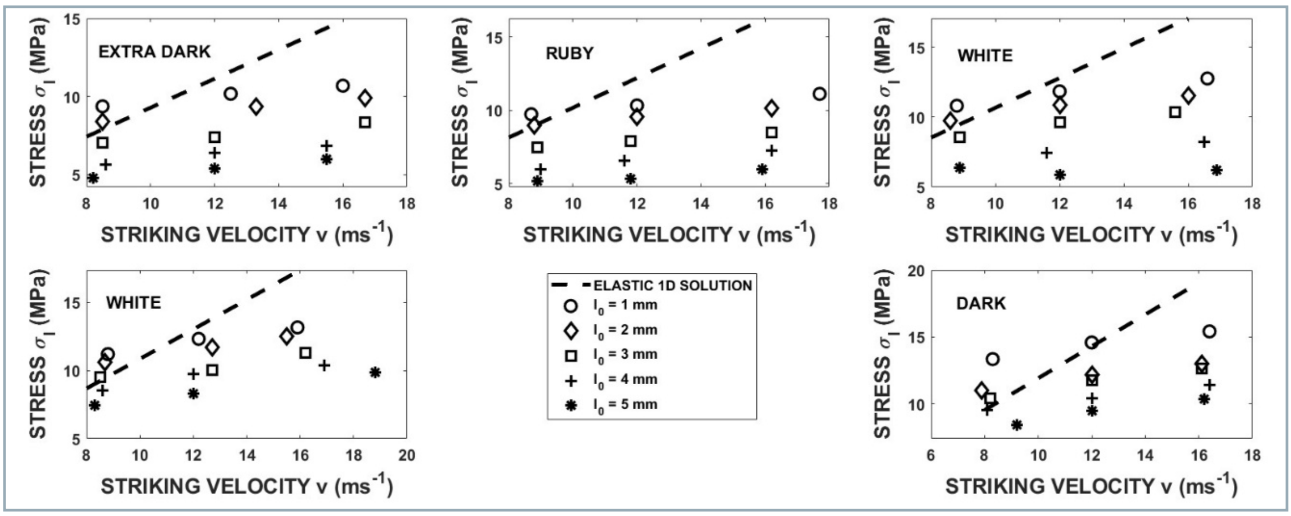

Fig. 7 The comparison of experimental data with the results of simplified 1D elastic model of bars impact

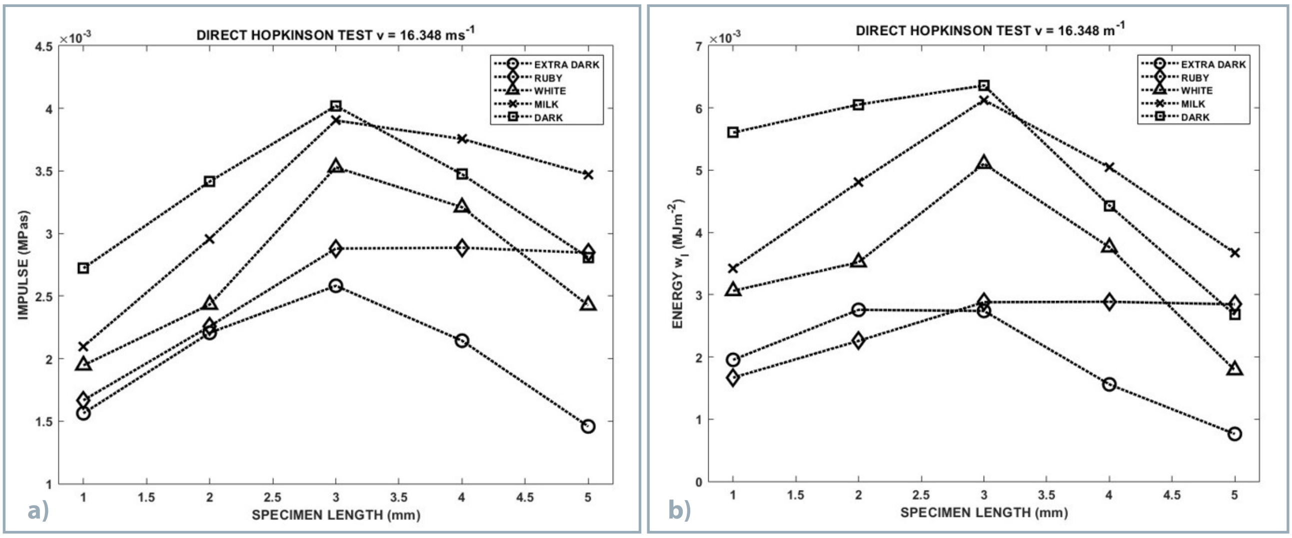

Fig. 8 a) The effect of the specimen length on the pulse impulse; b) The effect of the specimen length on the stress pulse energy

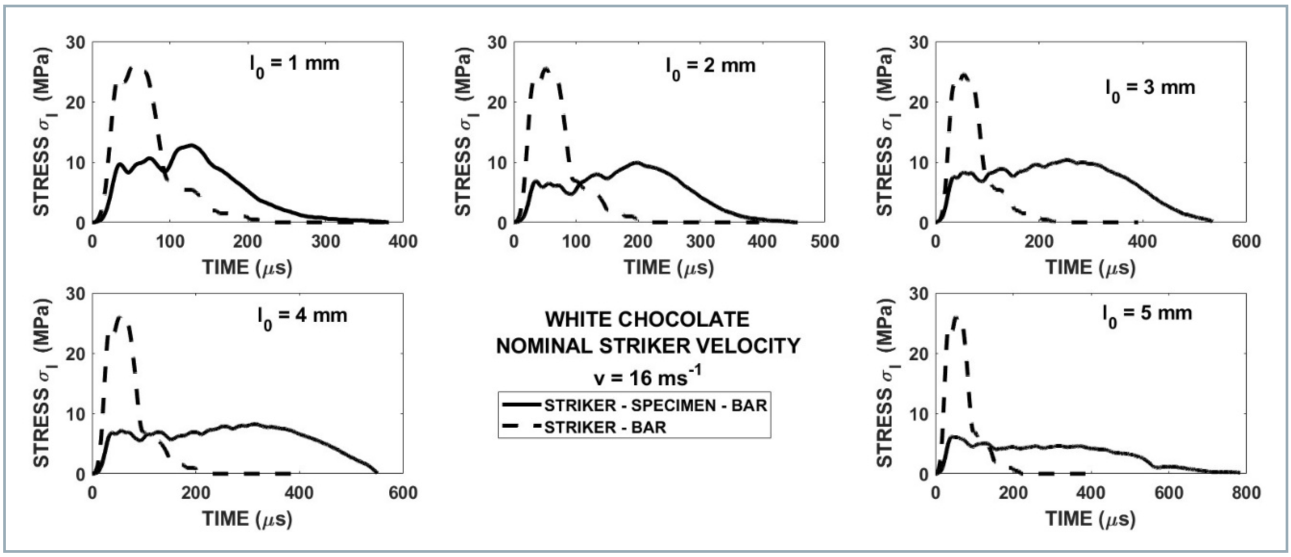

Fig. 9 The example of experimental records of stress pulses (broken line corresponds)

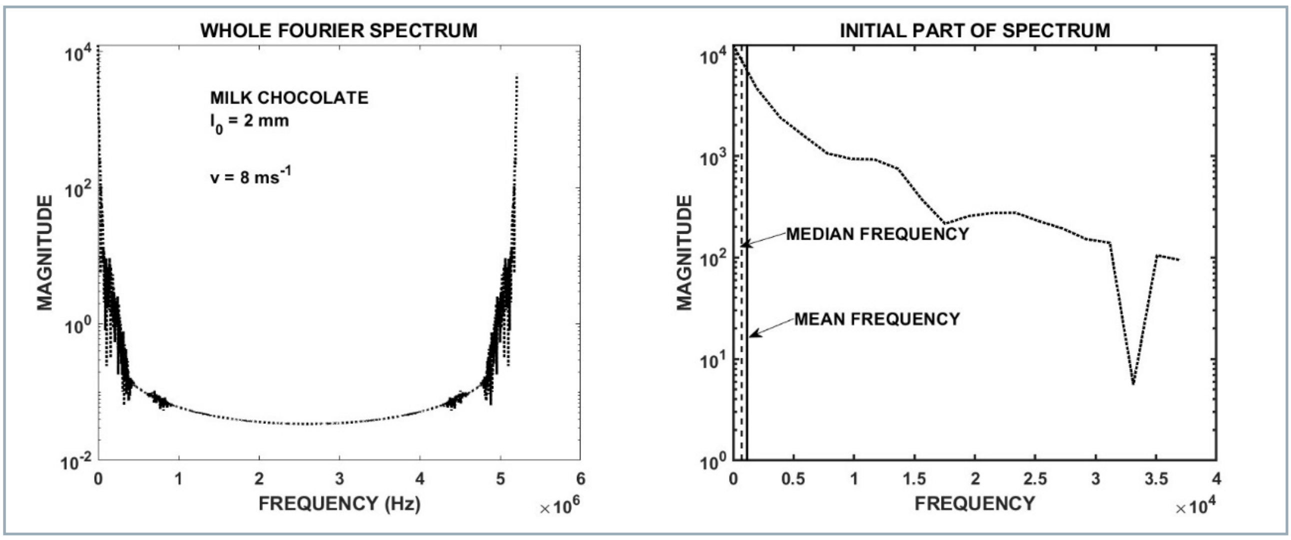

Fig. 10 The frequency dependence of the magnitude

This behaviour may be attributed to the evolution of the stress pulse shape during the interaction between the specimen and the impactor. Figure 9 illustrates an example of two stress pulses. The first pulse (depicted by the dashed line) corresponds to the impact of the striker on the elastic bar when no specimen is positioned between them. The second pulse (solid line) was recorded with the specimen placed between the striker and the elastic bar. It is evident that the plastic deformation of the specimen leads to significant alterations in the pulse shape. These changes vary with different specimen lengths and can be described by analysing the specimen's response in the frequency domain. This response is characterized by the spectral function defined in Eq. (16).

Figure 10 presents an example of the frequency dependence of the magnitude. The spectrum is symmetric, with the majority of its components concentrated within a narrow frequency band. The mean and median frequencies were employed to characterize this behaviour. The mean frequencies fmean are displayed in Fig. 11.

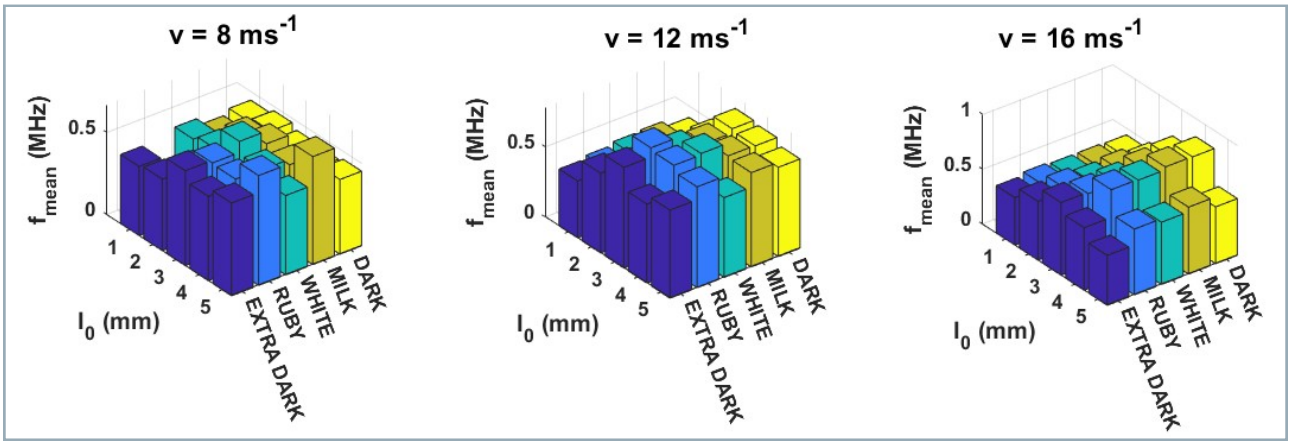

Fig. 11 The mean frequencies of the magnitude frequency distribution

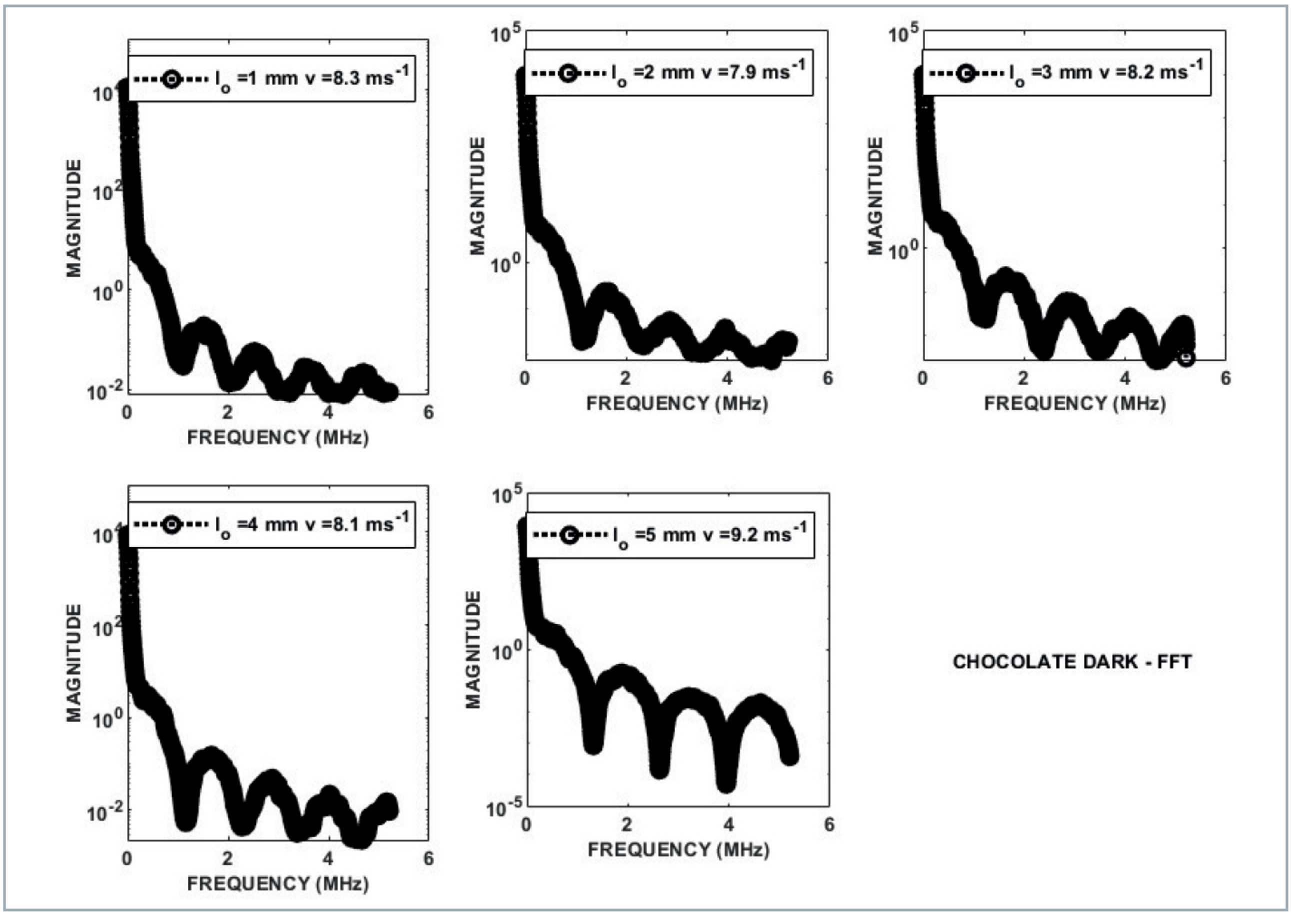

Fig. 12 The magnitude of the spectral function

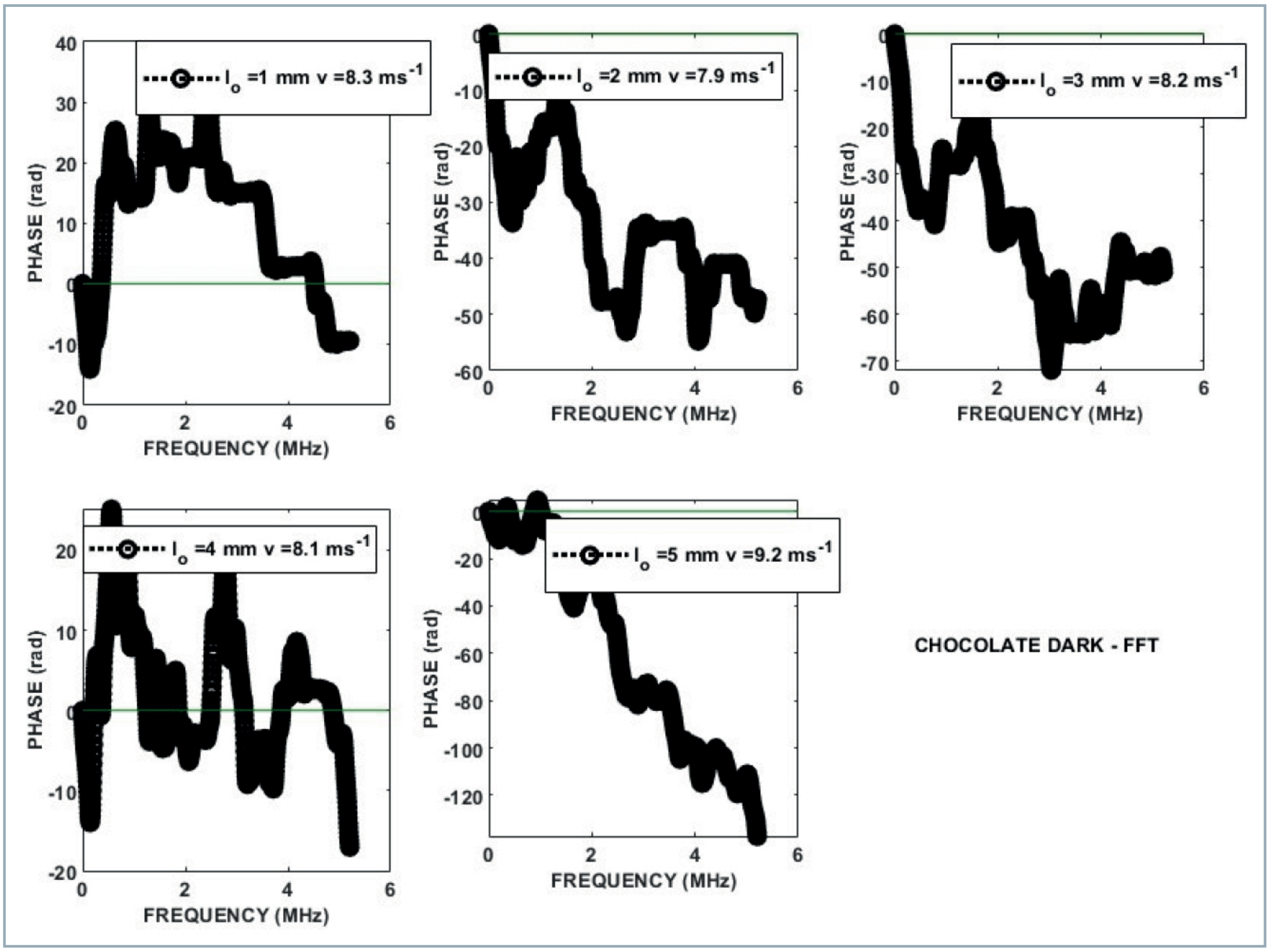

Fig. 13 The phase of the spectral function

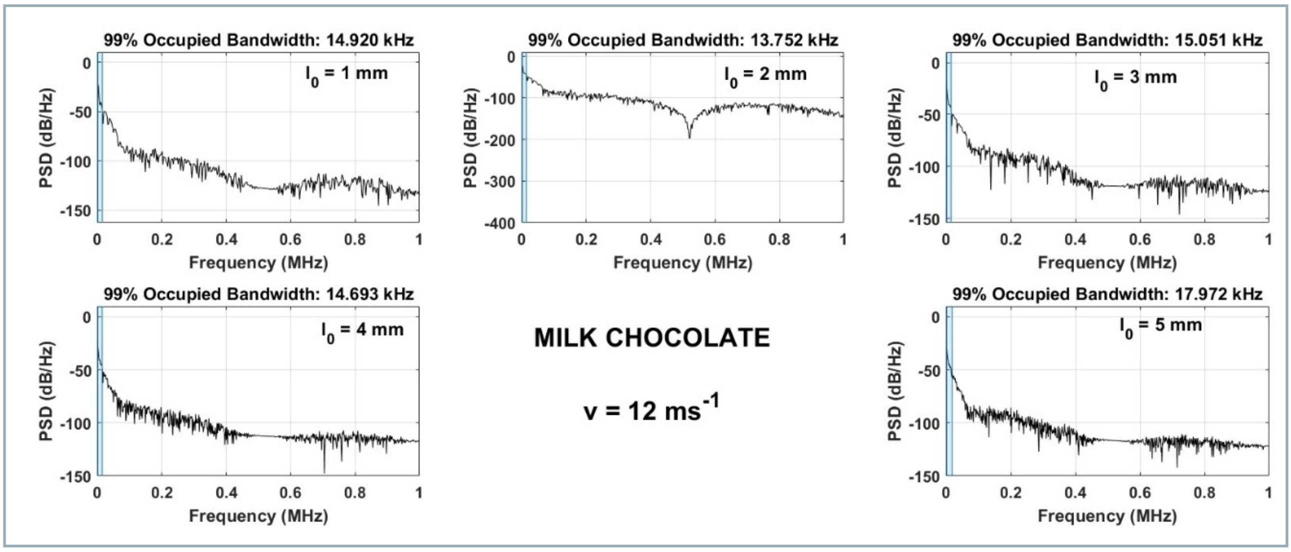

Fig. 14 Power spectrum density – example

An example of the magnitude's frequency dependence at frequencies lower than those presented in Fig. 10 is shown in Fig. 12.

Figure 13 illustrates the frequency dependence of the phase of the spectral function. The magnitude decreases significantly with increasing frequency. The qualitative features of this frequency dependence are consistent across all stress pulses. However, some differences can be observed in the frequency dependencies of the phase of the spectral functions.

An additional characteristic of the stress pulse is its power spectral density (PSD), which quantifies the distribution of power over frequency within the signal (stress pulse) (Stoica and Moses, 1997). The PSD is measured in the units of power per unit frequency, such as watts per hertz. The examples illustrating these PSD characteristics are presented in Fig. 14.

Analysis shows that the majority of the power is concentrated within a narrow frequency band, a conclusion that holds true for all tested chocolates. Figure 15 presents the power bandwidth (PBW), as defined by Stoica and Moses (1997), for all the chocolates examined. The results indicate that this quantity depends on both the specimen length and the striking velocity. Moreover, variations in PBW are observed among the different types of chocolates.

An additional characteristic of the spectral function is the average magnitude defined as:

$$\overline{P} = \frac{\sum_{i=0}^{n} P_i}{n+1} \tag{17}$$

where: P_i – the amplitude at the i^{th} frequency f_i in the frequency domain

Observations indicate that the average magnitude decreases with increasing specimen length and increases with the striking velocity v, which corresponds to the amplitude of the stress pulse (Fig. 16).

An inverse relationship is observed between the average amplitude and the specimen length. The ranking of the chocolates based on the average magnitude values corresponds to that determined by Eq. (15). Consequently, the average magnitude can be used to describe the stress pulse attenuation within the specimen.

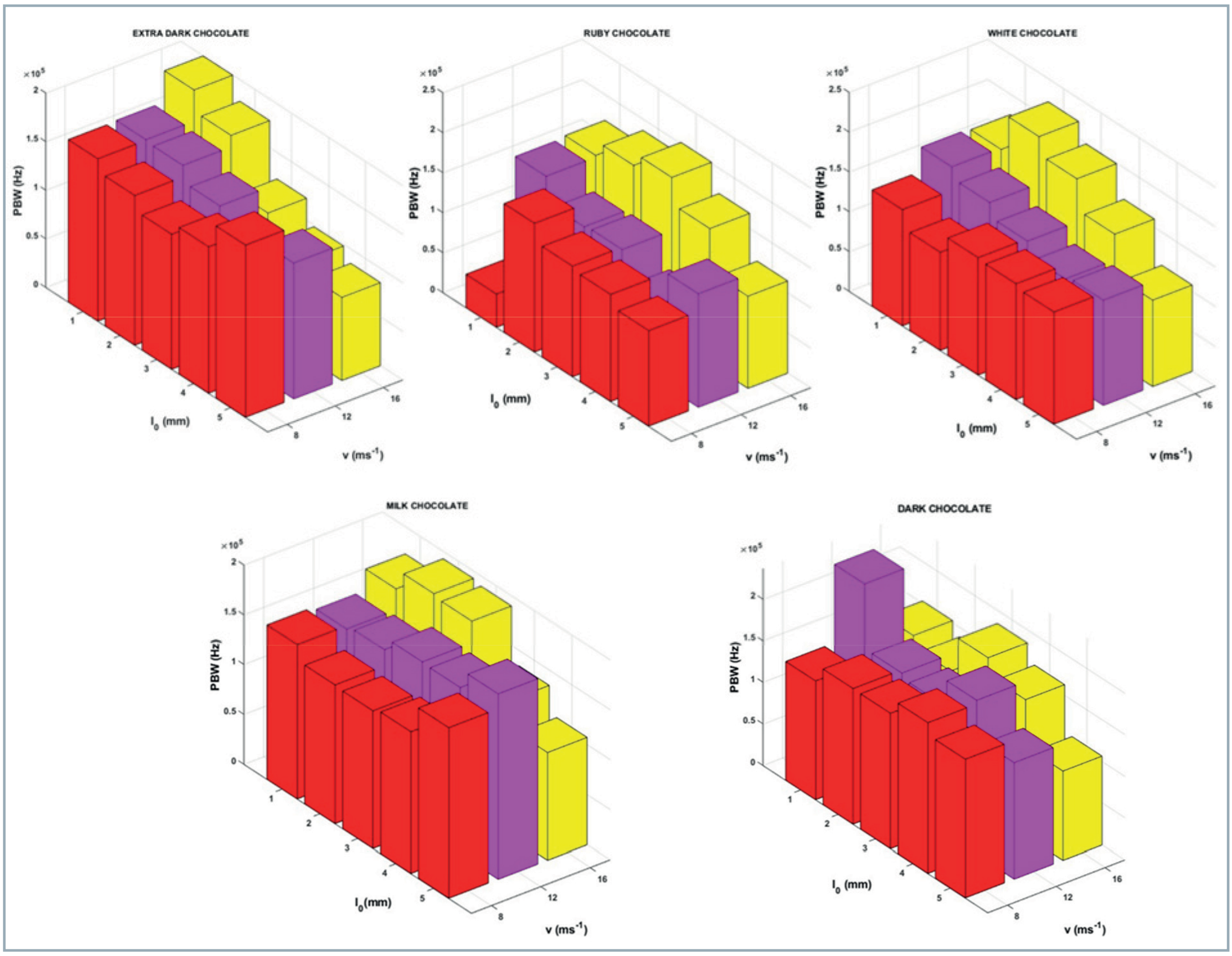

Fig. 15 The width of the power band (PBW)

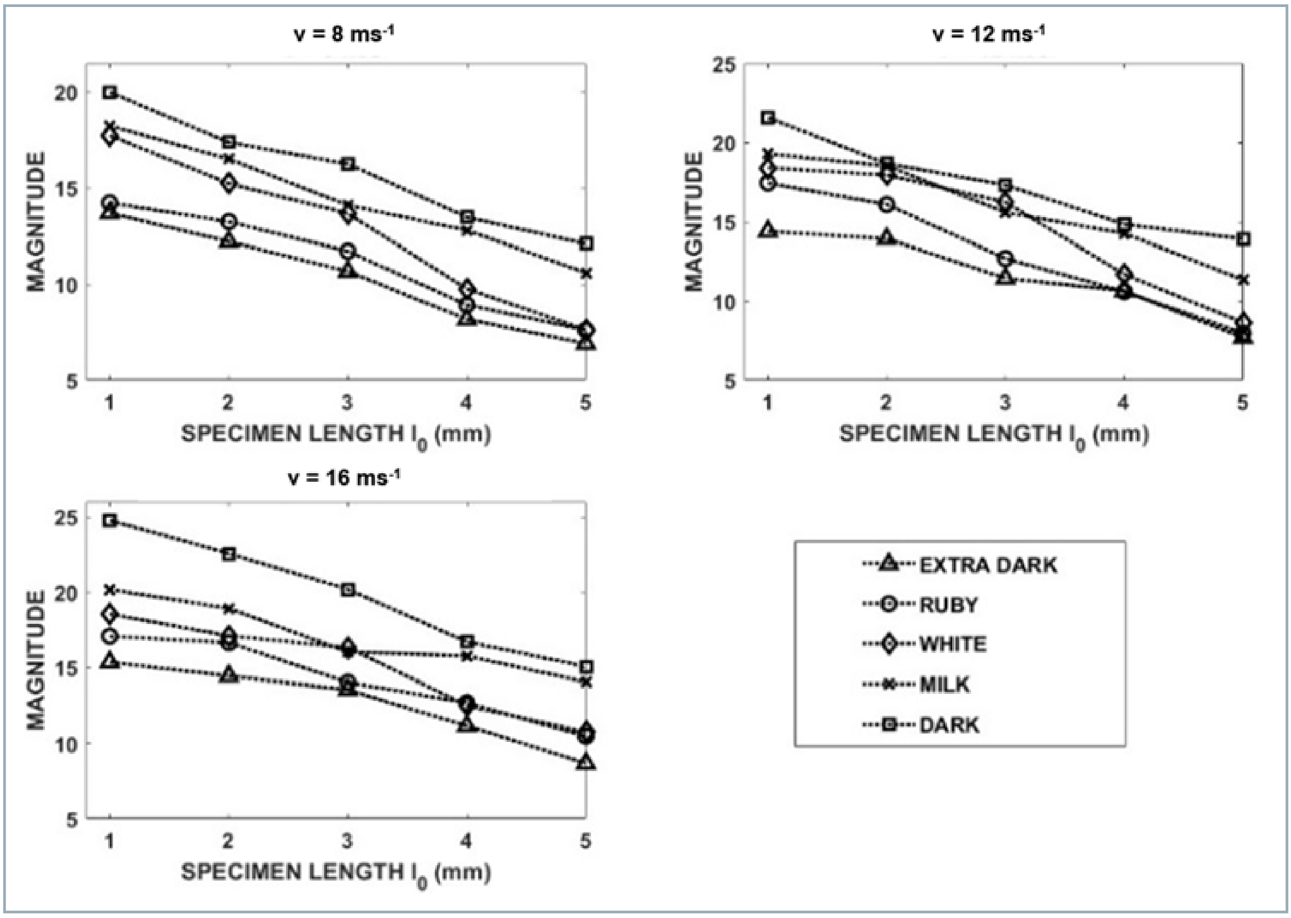

Fig. 16 The effect of the specimen length on the average magnitude

Conclusion

The chocolates exhibit significant stress attenuation, as characterized by the dependence of the stress pulse maximum (amplitude) on specimen length. For a given specimen length, the stress pulse amplitude increases with the striking velocity, indicating the strain-rate sensitivity of the tested chocolates. Results obtained using the Direct Impact Hopkinson Bar (DIHB) technique are qualitatively consistent with previous findings from the Split Hopkinson Pressure Bar (SHPB) technique. This suggests that the SHPB technique can be utilized to evaluate real impact processes similar to those realized by the DIHB technique. The specimen response can be described in both the time and frequency domains. Furthermore, the material's response to impact loading can also be predicted using the value of its acoustic impedance.

The DIHB and SHPB techniques can reflect the effect of chocolate processing, particle size distribution, and additive composition on the mechanical behaviour. This may be used to test the quality of chocolates and their defects. Also, the data obtained in this paper may be used for the numerical simulation of the chocolate behaviour at impact loading.

Acknowledgement

This research was funded by the FA MENDELU project no. AF-IGA-2020-TP006 and Czech Grant Agency project no. GF22-00863K.

References

BALDINO, N. – GABRIELE, D. – MIGLIORI, M. 2010. The influence of formulation and cooling rate on the reological properties of chocolate. In European Food Research and Technology, vol. 231, no. 6, pp. 821–828. DOI: https://doi.org/10.1007/s00217-010-1334-3

BIKOS, D. – SAMARAS, G. – CANN, P. – MASEN, M. – HARDALUPAS, Y. – HARTMANN, C. – VIEIRA, J. – CHARALAMBIDES, M. N. 2021. Effect of micro-aeration on the mechanical behaviour of chocolates and implications for oral processing. In Food and Function, vol. 12, no. 11, pp. 4826–4886. DOI: https://doi.org/10.1039/d1fo00045d

BIKOS, D. – SAMARAS, G. – CANN, P. – MASEN, M. – HARDALUPAS, Y. – VIEIRA, J. – HARTMANN, C. – HUTHWAITE, P. – LAN, B. – CHARALAMBIDES, M. N. 2023. Destructive and non-destructive mechanical characterisation of chocolate with different levels of porosity under various modes of deformation. In Journal of Materials Science, vol. 58, no. 11, pp. 5104–5127. DOI: https://doi.org/10.1007/s10853-023-08324-7

BHATTACHARYYA, T. – JOSHI, Y. M. 2022. Effect of thermal and mechanical rejuvenation on the rheological behavior of chocolate. In Physics of Fluids, vol. 34, no. 3, article no. 037111. DOI: https://doi.org/10.1063/5.0083335

CARVALHO-DA-SILVA, A. M. – VAN DAMME, I. – WOLF, B. – HORT, J. 2011. Characterisation of chocolate eating behaviour. In Physiology and Behavior, vol. 104, no. 5, pp. 929–933. DOI: https://doi.org/10.1016/j.physbeh.2011.06.001

COUQUE, H. 2014. The use of the direct impact Hopkinson pressure bar technique to describe thermally activated and viscous regimes of metallic materials. In Philosophical Transactions of the Royal Society A: Mathematical, Physical and Engineering Sciences, vol. 372, no. 2023, article no. 20130218. DOI: https://doi.org/10.1098/rsta.2013.0218

GLICERINA, V. – BALESTRA, F. – DALLA ROSA, M. – ROMANI, S. 2013. Rheological, textural and calorimetric modifications of dark chocolate during process. In Journal of Food Engineering, vol. 119, no. 1, pp. 173–179. DOI: https://doi.org/10.1016/j.jfoodeng.2013.05.012

GÓMEZ, F. J. – SALAZAR, A. – MARTÍNEZ, M. – RANA, S. K. – RODRÍGUEZ, J. 2022. Fracture of notched samples of chocolate. In Theoretical and Applied Fracture Mechanics, vol. 121, article no. 103477. DOI: https://doi.org/10.1016/j.tafmec.2022.103477

GUO, X. – HEUZÉ, T. – OTHMAN, R. – RACINEUX, G. 2014. Inverse identification at very high strain rate of the Johnson-Cook constitutive model on the Ti-6Al-4V alloy with a specially designed direct-impact Kolsky bar device. In Strain, vol. 50, no. 6, pp. 527–538. DOI: https://doi.org/10.1111/str.12114

HENDRIK, N. J. – MARCHESINI, F. H. – VAN DE WALLE, D. – DEWETTINCK, K. 2023. Accurate evaluation of the flow properties of molten chocolate: Circumventing artefacts. In Food Analytical Methods, vol. 16, no. 1, pp. 190–205. DOI: https://doi.org/10.1007/s12161-022-02406-z

KIUMARSI, M. – RAFE, A. – YEGANEHZAD, S. 2017. Effect of different bulk sweeteners on the dynamic oscillatory and shear rheology of chocolate. In Applied Rheology, vol. 27, no. 6, article no. 64123. DOI: https://doi.org/10.3933/APPLRHEOL-27-64123

KUMBÁR, V. – KOUŘILOVÁ, V. – DUFKOVÁ, R. – VOTAVA, J. – HŘIVNA, L. 2021. Rheological and pipe flow properties of chocolate masses at different temperatures. In Foods, vol. 10, no. 11, article no. 2519. DOI: https://doi.org/10.3390/foods10112519

KUMBÁR, V. – TRNKA, J. – KOUŘILOVÁ, V. – DUFKOVÁ, R. – VOTAVA, J. – NEDOMOVÁ, Š. – HŘIVNA, L. – POLCAR, A. – BUCHAR, J. 2023. High strain rate behaviour of different types of chocolate. In Journal of Food Engineering, vol. 346, article no. 111438. DOI: https://doi.org/10.1016/j.jfoodeng.2023.111438

KUMBÁR, V. – TRNKA, J. – KOUŘILOVÁ, V. – DUFKOVÁ, R. – VOTAVA, J. – ČUPERA, J. – NEDOMOVÁ, Š. – HŘIVNA, L. – BUCHAR, J. 2024. Stress wave attenuation in chocolate. In Journal of Food Engineering, vol. 374, article no. 112037. DOI: https://doi.org/10.1016/j.jfoodeng.2024.112037

LE RÉVÉREND, B. – SAUCY, F. – MOSER, M. – LORET, C. 2016. Adaptation of mastication mechanics and eating behaviour to small differences in food texture. In Physiology & Behavior, vol. 165, pp. 136–145. DOI: https://doi.org/10.1016/j.physbeh.2016.07.010

MARKOVSKY, P. E. – JANISZEWSKI, J. – STASIUK, O. O. – SAVVAKIN, D. G. – ORYSHYCH, D. V. – DZIEWIT, P. 2023. Mechanical energy absorption ability of titanium-based porous structures produced by various powder metallurgy approaches. In Materials, vol. 16, no. 9, article no. 3530. DOI: https://doi.org/10.3390/ma16093530

MOHAMAD, N. J. – GRAY, D. – WOLF, B. 2020. Spinach leaf and chloroplast lipid: A natural rheology modifier for chocolate? In Food Research International, vol. 133, article no. 109193. DOI: https://doi.org/10.1016/j.foodres.2020.109193

NEDOMOVÁ, Š. – TRNKA, J. – BUCHAR, J. 2013. Tensile strength of dark chocolate. In Acta Technologica Agriculturae, vol. 16, no. 3, pp. 71–73. DOI: https://doi.org/10.2478/ata-2013-0018

NEDOMOVÁ, Š. – TRNKA, J. – KOUŘILOVÁ, V. – DUFKOVÁ, R. – VOTAVA, J. – HŘIVNA, L. – KUMBÁR, V. – BUCHAR, J. 2023. Acoustic properties and low strain rate behavior of different types of chocolate. In International Journal of Food Properties, vol. 26, no. 1, pp. 842–854. DOI: https://doi.org/10.1080/10942912.2023.2189087

SHUI-SHENG, Y. – YU-BIN, L. – YONG, C. 2013. The strain rate effect of engineering materials and its unified model. In Latin American Journal of Solids and Structures, vol. 10, no. 4, pp. 833–844. DOI: https://doi.org/10.1590/s1679-78252013000400010

STEIN, E. M. – SHAKARCHI, R. 2003. Fourier Analysis: An introduction. New Jersey (U.S.) : Princeton University Press, 328 pp. ISBN 0-691-11384-X

STOICA, P. – MOSES, R. L. 1997. Introduction to Spectral Analysis. New Jersey (U.S.): Prentice Hall, 319 pp. ISBN 0-132-58419-0

TALANSIER, E. – BACCONNIER, A. – CATON, F. – CHASTEL, C. – COSTA, L. – GUNES, D. Z. – ROUX, D. C. D. 2019. Accurate methodology to determine slip velocity, yield stress and the constitutive relation for molten chocolate. In Journal of Food Engineering, vol. 244, pp. 220–227. DOI: https://doi.org/10.1016/j.jfoodeng.2018.09.031

WANG, W. – YANG, J. – DENG, G. Q. – CHEN, X. 2023. Theoretical analysis of stress equilibrium of linear hardening plastic specimen during SHPB tests. In Experimental Mechanics, vol. 63, no. 8, pp. 1353–1369. DOI: https://doi.org/10.1007/s11340-023-00994-3

ZHAO, H. – LI, B. – JAMES, B. J. 2018. Structure-fracture relationships in chocolate systems. In LWT, vol. 96, pp. 281–287. DOI: https://doi.org/10.1016/j.lwt.2018.05.045